Audio Engineering Society

Convention Paper 10206

Presented at the AES 158th Convention
2025 May 22–24, Warsaw, Poland

This paper was peer-reviewed as a complete manuscript for presentation at this convention. This paper is available in the AES E-Library (http://www.aes.org/e-lib), all rights reserved. Reproduction of this paper, or any portion thereof, is not permitted without direct permission from the Journal of the Audio Engineering Society.

Mixed-Phase Equalization of Slot-loaded Impulse Responses

Sunil Bharitkar[1] and William Decanio[1]

[1]*DMS Audio Lab, Samsung Research America*

Correspondence should be addressed to Sunil Bharitkar (s.bharitkar@samsung.com)

ABSTRACT

This paper introduces a new algorithm for multiposition mixed-phase equalization of slot-loaded loudspeaker responses obtained in the horizontal and vertical plane, using finite impulse response (FIR) filters. The algorithm selects a *prototype response* that yields an equalization filter from optimization of a time-domain-based objective metric for a given plane. The objective metric includes a weighted linear combination of pre-ring energy, early and late reflection energy, and decay rate (characterizing impulse response shortening) during filter synthesis. The results show that the presented mixed-phase multiposition filtering algorithm performs a good equalization along all horizontal directions and for most positions in the vertical direction. Beyond the multiposition filtering capabilities, the algorithm and the metric are suitable for designing mixed-phase filters with low delays, an essential constraint for real-time processing.

1 Introduction

The traditional loudspeaker design process involves properly selecting drivers with a sufficiently smooth amplitude response over the desired bandwidth and designing an enclosure with good low-frequency extension. In the case of slim form-factor consumer devices such as TVs, acoustic radiation from the transducer may be coupled to the room through a slot or aperture wherein the transducer resides. This coupling causes degradations in the measured time and magnitude response.

Accordingly, equalizing loudspeakers in an enclosure delivers high-quality audio to support mono-channel and various ITU recommendation formats [1]. Conventional equalization involves initially deconvolving the loudspeaker-enclosure response $h(n)$ after energizing a loudspeaker with excitation stimuli such as sweep, maximum-length sequence, perfect sequence ([2], [3], [4], [5], [6], etc.) and then designing a minimum-phase equalization filter to pre-process the audio sent to the loudspeaker for reproduction. For an objectively transparent result, where the signal at the microphone location i is the same as the signal to the input of the equalization filter, the requirement $w(n) \otimes h_i(n) = \delta_i(n-\Delta)$ where $\otimes$ is the linear convolution operator needs to be satisfied. As can be seen through an example depicted in Fig. 1, this requirement is not met by a minimum-phase filter designed from $h_2(n)$ Fig. 1(a) & (c), nor at a neighboring position response $h_1(n)$ Fig. 1 (b) & (d). Specifically, in both (a) & (b) the convolution with $h^{-1}_{\text{mineq},2}(n)$ does not "shorten" the equalized response of $h_2(n)$ or $h_1(n)$ to approximate $\delta(n-\Delta)$. Several techniques can approximate a delta function for single- or multi-position equalization. Such algorithms can leverage either non-parametric (least-squares or Fourier inversion) (e.g., [7], [8], [9] etc.) or parametric autoregressive-based models (e.g., [12], [13], etc.). A summary of loudspeaker-room equalization

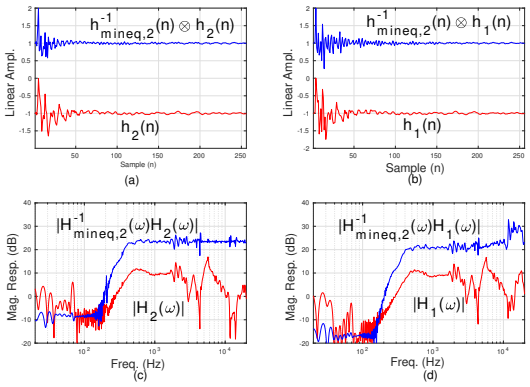


Fig. 1: Minimum-phase filtering performance over two positions (red-bottom: original, blue-top: equalized).

and techniques can be found in various publications (e.g., [10], [11]). In the context of mixed-phase filtering, single-position transient equalization is presented in [14] based on least-squares error minimization of an error using an all-pole model. Greenfield *et al.* [15] present an IIR model of order 40 and 50 to achieve temporal equalization at one position. Elliott *et al.* [16] present a multi-position mixed-phase adaptive filter designed over four positions that minimize the mean-square error. The filtering performance exhibits pre-echoes and limited suppression of post-echoes over the positions (see Fig. 10 in [16]). Use of Levinson and Simpson sideways recursion for model-based loudspeaker driver equalization using a least-squares error (with on- and off-axis responses) in the horizontal direction at three angles (on-axis at $0^\circ, 10^\circ$ and 30°) is presented in [17]. The results show good performance for on-axis and adjacent 10° but limited IR shortening with less suppression of post-echoes at 30° (see Fig. 18 in [17]). Mourjopoulos [18] presents an all-pole vector quantization (VQ) based filter premised on minimizing the spectral deviations in the magnitude response. Additional techniques with mixed-phase filters can be found in [19]-[36].

The key contributions of this paper are: (i) a new multi-position transient response correction algorithm using mixed-phase filter design, (ii) a new multi-position optimization metric used by the algorithm that includes weighted combinations of energies from different parts of the impulse response and a temporal shortening function to determine the best mixed-phase filter, (iii) improvement of the iterative decomposition [9] and incorporating a delay (Δ) search technique used in the algorithm by using the optimization metric. Towards validating the performance, this paper also uses a large number of measurements (seventeen in each horizontal and vertical direction) for two different slot-loaded drivers from TVs, thereby creating a diverse measurement dataset. As a byproduct, the algorithm can generate suitable candidate filters with low delays for real-time processing. Finally, the algorithm can be readily adapted to correct the in-room temporal response with loudspeakers.

The paper's organization is as follows. Section 2 provides the iterative decomposition background, whereas Section 3 discloses the measurement setup for the slot transducers, along with examples of impulse responses in each horizontal and vertical plane. Section 4 details the algorithm and the objective metric for designing the mixed-phase filter. Section 5 presents the results associated with the filter performance, whereas Section 6 summarizes the paper and proposes future research directions.

2 Approximate Minimum-phase and All-pass Iterative Decomposition

Radlovic *et al.* [9] presented an iterative decomposition technique for minimum-phase and all-pass separation of an impulse response (viz., $h(n) = h_{mp}(n) \otimes h_{ap}(n)$ to overcome the limitations of using homomorphic transformation involving cepstral analysis [37] (pp. 768–771)). For example, in the case of ill-conditioned non-minimum phase responses (as pertinent to loudspeaker-coupled measurements), the cepstral approach could lead to an inaccurate estimate of $h_{ap}(n)$, given the finite-point nature of Discrete Fourier Transform (DFT) algorithms. In essence, the computation of the all- pass sequence is inaccurate due to time aliasing in the circular convolution of the sequences $h(n)$ and $h_{mp}^{-1}(n)$ [37] (pp. 542–546), [9]. Thus, an iterative decomposition involving a sequential flattening of the logarithmic magnitude response was used in each iteration r for single-position equalization [9]. The iteration process is repeated through an upper limit $r = L$ until the amplitude spectrum deviation is below a desired threshold. Equations (1) govern the iterative decomposition of the minimum phase and all-pass

component.

$$
\begin{aligned}
H_i(k) &= \mathscr{F}\{h_i(n)\} = \sum_{n=0}^{N-1} h_i(n) e^{-j(2\pi/N)kn} \\
\hat{h}_{e,i}(n) &= \frac{1}{N} \sum_{k=0}^{N-1} \log|H_i(k)| e^{j(2\pi/N)kn} \\
\hat{h}_{mp,i}(n) &= \begin{cases} \hat{h}_{e,i}(n), & n = 0, N/2 \\ 2\hat{h}_{e,i}(n) & 1 \le n < N/2 \\ 0 & N/2 < n \le N-1 \end{cases} \\
\hat{H}_{mp,i}(k) &= DFT\{\hat{h}_{mp,i}(n)\} \\
\hat{H}^{(r)}_{mp,i}(k) &= \hat{H}_{mp,i}(k)/2^{r+1}; \qquad (1a) \\
H^{(r)}_{mp,i}(k) &= \exp[\hat{H}^{(r)}_{mp,i}(k)] \qquad (1b) \\
H^{(r+1)}_{i}(k) &= H^{(r)}_{i}(k)/H^{(r)}_{mp,i}(k) \qquad (1c) \\
H^{(0)}_{i}(k) &= H_i(k)
\end{aligned}
$$

Equations (1a)-(1c) are iterated in a loop while $r \le L$. As an extension, in this paper, we determine the optimal number of iterations L by employing a time-domain metric in the multi-position equalization algorithm described in Sec. 4.

3 Measurement of Slot-loaded Loudspeakers

Figure 2a shows the two slot-loaded device under test (DUT) used in this study (viz., DUT-1 in the top panels and DUT-2 in the bottom panels, respectively) where the arrow next to the DUT-1 shows the location of the slot. The figure shows the mounting in the 2π baffle (middle column) for measurements in the anechoic chamber (right column). Custom made fixtures were used to mount the transducer systems such that the ends of their respective slots were flush with the inside surface of the chamber baffle/wall. A stimulus level of 1.5 volts rms was selected to balance transducer linearity versus measurement signal to noise ratio. The microphones used are positioned along an arc shaped boom 1.8m from the measurement baffle center and the sound pressure level was normalized to 1m. Figure 2b highlights the horizontal and vertical sampling space for the impulse response measurements for each slot. Specifically, there are seventeen measurements in each horizontal and vertical direction for thirty-four measurement points for each transducer. A logarithmic sweep stimulus at $f_s = 48$ kHz sampling frequency deconvolves the transducer slot impulse responses. Due to space limitations, a subset (viz. six of seventeen



(a) **(b)**

Fig. 2: (a) Top row slot DUT-1, bottom row DUT-2 and associated 2π baffle anechoic measurement setup Geometric representations for determining microphone-source angles (b) Measurement setup for each slot (seventeen measurement points in the horizontal and vertical plane)

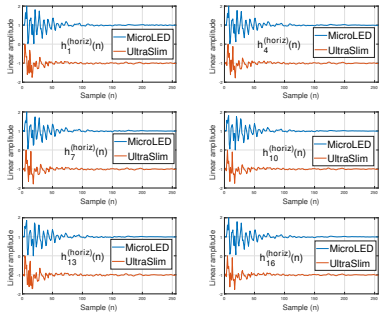


Fig. 3: Example six of seventeen horizontal impulse responses (blue: DUT-1, orange: DUT-2).

responses) for each of the horizontal and vertical positions of the impulse responses is shown in Figs. 3-4. For both transducers, there are some variations in the impulse responses in the horizontal plane between positions (relative to the vertical measurements). In contrast, these variations are more prominent between positions in the vertical plane due to the directivity effect of the longer slot dimension.

4 Algorithm for Mixed-phase Filter Synthesis with Weighted Temporal Metric

As detailed in Sect. 4.1 and 4.2, the proposed algorithm assesses each slot impulse response, $h_i(n)$ in the measurement set (for a given horizontal or vertical plane) as a *prototype candidate* for generating a time-domain filter $w^{(P)}_{i,\Delta,L}(n)$ with order P. This algorithm uses (i)

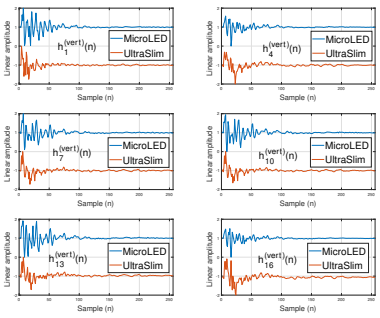


Fig. 4: Example six of seventeen vertical impulse responses (blue: DUT-1, orange: DUT-2).

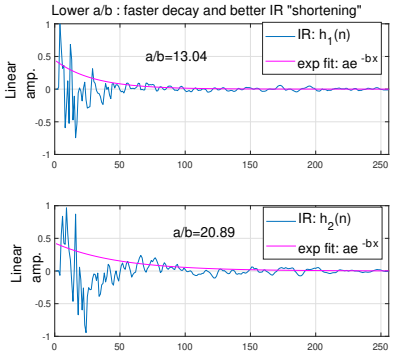


Fig. 5: Impulse response (IR) and its exponential decay fit (modeling "spreading/shortening" of IR).

an incremental search for the optimal number of iterations L to use in iterative decomposition for minimum-phase and a causal all-pass filter and (ii) an incremental search for the delay (Δ) applied to the inverted all-pass filter. The algorithm incorporates a weighted temporal metric to identify the optimal delay Δ^* and iteration L^* for the filter generated from the given prototype candidate $h_i(n)$. The metric determines the quality of improvement (or degradation) by first computing the difference between the energies in various parts of the original response ($h_m(n)$) and the equalized responses ($w^{(P)}_{i,\Delta,L}(n) \otimes h_m(n)$) for all positions $m \in \{1,2,\ldots,M\}$. The process is repeated over all candidate prototypes $h_j(n)$ with $1 \leq j \leq M$), and the best filter $w^{(P)}_{i^*,\Delta^*,L^*}(n)$ is selected that maximizes the metric.

4.1 Temporal Weighted Metric

It is well known that mixed-phase filtering can introduce pre- and post-echoes in the equalized responses [7], [18]. These arise due to several factors, including (i) mismatch between the impulse responses at two different positions (viz., a mixed-phase filter designed in one position but applied to another position), (ii) truncation effects on the all-pass components due to constraining the length of the FIR filter, and (iii) equalizing high Q notches. The proposed metric incorporates the energy in the (a) pre-echoes, (b) post-echoes (comprising early and late energy of the reflections), and (c) a measure of the decay rate of the impulse response. These four terms are linearly weighted with different coefficients to obtain a trade-off in the equalized responses during filter synthesis. The temporal metric as a measure of performance at a given position m, for a *unit-amplitude normalized* response $h_m(n)$, is expressed as,

$$\begin{aligned} \tau(m) &= \alpha_1 \|h_m(n)\|^{\text{pre}} + \alpha_2 \|h_m(n)\|^{\text{early}} \\ &+ \alpha_3 \|h_m(n)\|^{\text{late}} + \alpha_4 a^{(m)}/b^{(m)} \end{aligned} \quad (2)$$

where the pre-echo energy is computed from $n = 0$ through $n = K$ for $|h(K)| \leq T$, the energy in the early part of the response is computed from $n = K+1$ through $n = Q$. The late energy is computed from $n = Q+1$ through the end of the response. The values of a and b are the y-intercept and the decay rate of an exponential fit ae^{-bx} to the impulse response $|h_m(n)|$. The faster the decay, the lower the value of a/b, hence a lower $\tau(m)$ compared to a slower decay impulse response with a higher $\tau(m)$. Fig. 5 shows comparisons where the top subplot (faster decay and better "shortening") is associated with a lower a/b value.

4.2 Algorithm

The core parameters that determine the equalization filter $w^{(P)}_{i,\Delta,L}(n)$ for a given prototype $h_i(n)$ include the iterative decomposition parameter L and the filter delay Δ. Consequently, a guided search employing a weighted temporal metric determines these parameters for a given prototype. The Algorithm describes the technique, where an impulse response $h_i(n)$ in the measurement set $\{h_m(n) : m = 1,\ldots,M\}$ is selected as a prototype candidate. For a given number of iterations, L, iterative decomposition (1) is used to obtain the minimum phase filter $G^L_{mp,i}(k)$ and the all-pass component

$H_i^{(L+1)}(k)$ for the frequency bin k. A candidate filter is generated for a given delay Δ and iteration L (line 9) by delaying the all-pass component by Δ after the conjugation operation. The measurements are delayed equally by Δ (viz., $q_\Delta^{(m)}(n)$, line 10) to time-align with the equalized response $f_{i,\Delta,L}^{(m)}(n)$ (line 11) before using the metric (line 12) to determine the quality of the filter. The optimal filter is then determined (line 20) after evaluating all prototypes with the sequential combinations of L and Δ. Towards multiposition equalization, the proposed temporal metric $\kappa_\Delta(m)$ (3) is computed for each position with a delay Δ . Similarly, a metric $\phi_{i,\Delta,L}(m)$ (3) is computed with the equalization filter $w_{i,\Delta,L}^{(P)}(n)$ (line 9) for each position and each prototype $h_i(n)$ ($i = 1,\ldots,M$). The metric computes energies in the pre-echoes, early and later part of the responses and shortening,

$$\begin{aligned}
\kappa_\Delta(m) &= \alpha_1\|q_\Delta^{(m)}(n)\|^{\text{pre}} + \alpha_2\|q_\Delta^{(m)}(n)\|^{\text{early}} \\
&+ \alpha_3\|q_\Delta^{(m)}(n)\|^{\text{late}} + \alpha_4 a_\Delta^{(m)}/b_\Delta^{(m)} \\
\phi_{i,\Delta,L}(m) &= \alpha_1\|f_{i,\Delta,L}^{(m)}(n)\|^{\text{pre}} + \alpha_2\|f_{i,\Delta,L}^{(m)}(n)\|^{\text{early}} \\
&+ \alpha_3\|f_{i,\Delta,L}^{(m)}(n)\|^{\text{late}} + \alpha_4 c_{i,\Delta,L}^{(m)}/d_{i,\Delta,L}^{(m)} \quad (3)
\end{aligned}$$

The difference in energies, β_m (4)in the various parts of the unequalized and equalized impulse response is then computed and sent through a sign function and summed to determine the number of positions where the equalized responses outperform the unequalized responses (expressed as $\lambda_{i,\Delta,L}$). Finally, λ is scaled by the sum of values conditioned where the equalized result is better ($\sum_{m=1}^{M}\beta_m|_{\text{sgn}(\beta_m)=1}$) to yield a composite multiposition measure $\psi_{i,\Delta,L}$. Thus, the higher the number of positions λ and the value β (where equalized responses are better), the higher this measure. In the extreme when $\beta_m < 0, \forall m \rightarrow \lambda = 0$, whereas when $\beta_m \geq 0, \forall m \rightarrow \lambda = M$. Accordingly, maximizing $\psi_{i,\Delta,L} \geq 0$ in (5) yields the optimal values of $\{i^*, \Delta^*, L^*\}$.

$$\begin{aligned}
\beta_m &= (\kappa_\Delta(m) - \phi_{i,\Delta,L}(m)) \\
\lambda_{i,\Delta,L} &= \sum_{m=1}^{M}(\frac{1}{2} + \frac{1}{2}\text{sgn}(\beta_m)) \\
\text{sgn(x)} &= \begin{cases} 1 & \text{if } x \geq 0 \\ -1 & \text{otherwise} \end{cases} \\
\psi_{i,\Delta,L} &= \lambda_{i,\Delta,L}(\sum_{m=1}^{M}\beta_m|_{\text{sgn}(\beta_m)=1}) \qquad (4)
\end{aligned}$$

Algorithm: Multi-position transient response equalization

Result: Filter: $w_{i^*,\Delta^*,L^*}^{(P)}(n)$ optimized over Δ, L and $i-$th prototype IR of order P

1 Initialize: Select $i = 1$, IR $h_i(n)$ candidate prototype $i \in \{1,\ldots,M\}$ with M measurement points $m = \{1,\ldots,M\}$, set $L \in \{1,\ldots,L^{up}\}$ (number of iterations for iterative decomposition);
2 **while** $i \leq M$ **do**
3 Select $i-$th candidate prototype IR $h_i(n)$, $L = 1$;
4 **while** $L \leq L^{up}$ **do**
5 Use iterative decomposition in Eq. (1) to compute minimum-phase inversion $G_{mp,i}^{(L)}(k) = 1/[H_{mp,i}^{(0)}(k)H_{mp,i}^{(1)}(k)\ldots H_{mp,i}^{(L-1)}(k)]$ and all-pass filter $H_i^{(L+1)}(k)$;
6 $\Delta = 1$;
7 **while** $\Delta \leq P/2$ **do**
8 With $*$ denoting complex conjugation, and $\otimes$ denoting linear convolution;
9 $w_{i,\Delta,L}^{(P)}(n) = \mathscr{F}^{-1}\{G_{mp,i}^{(L)}(k)H_i^{*(L+1)}(k)e^{-j(2\pi/N)kn\Delta}\}$;
10 $q_\Delta^{(m)}(n) = \mathscr{F}^{-1}\{H_m(k)e^{-j(2\pi/N)kn\Delta}\}, \forall m$;
11 $f_{i,\Delta,L}^{(m)}(n) = w_{i,\Delta,L}^{(P)}(n) \otimes h_m(n), \forall m$;
12 Compute $\kappa_\Delta(m)$ and $\phi_{i,\Delta,L}(m); \forall m$ using (3);
13 $\Delta = \Delta + 1$;
14 **end**
15 $L = L + 1$;
16 **end**
17 Compute (4);
18 $i = i + 1$;
19 **end**
20 Per (5), select $w_{i^*,\Delta^*,L^*}^{(P)}(n)$ that maximizes (4) ;

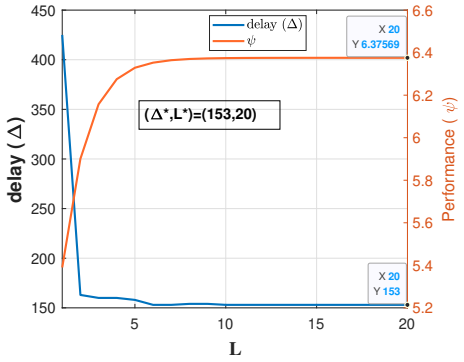


Fig. 6: Filter design parameters (L,Δ) to maximize ψ.

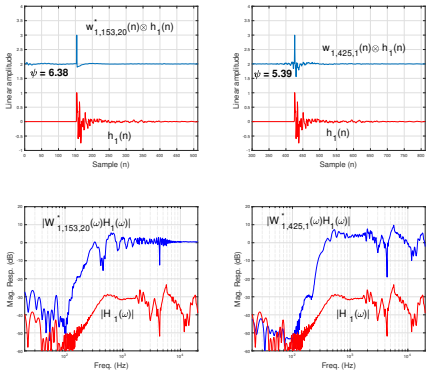


Fig. 7: Filtering performance with single filter at two different L and Δ (red-bottom: original, blue-top: equalized).

$$\max_{i,\Delta,L} \psi_{i,\Delta,L} \rightarrow (i^*,\Delta^*,L^*) \tag{5}$$

A depiction of the mechanism of the metric, as an example, for a single position response $h_1(n)$ is shown in Figs. 6-8. Specifically, Fig. 6 shows ψ on the right y-axis (orange curve) and Δ on the left y-axis (blue curve) using the response $h_1(n)$ shown as a bottom red plot in the top panel of Fig. 7. The filter order is set to $P = 512$. The value $\psi^* = 6.37$ is obtained using the orange curve at $L = 20$, and the delay obtained at this L is $\Delta = 153$ samples. The result from the optimal equalization filter $w^{(512)}_{1,153,20}(n)$ is shown in the top blue plot (in the top left panel). As evidence, besides significant shortening (fast decay), there are no pre- or post-echoes. The bottom left panel shows the corresponding magnitude responses. A filter designed with sub-optimal parameters ($\Delta = 425, L = 1$ with $\psi = 5.39$) results in pre- and post-echoes and less shortening, as shown in the top right panel's blue curve. Furthermore, if the optimal single-position-designed equalization filter, $w^{(512)}_{1,153,20}(n)$, is convolved with the response at position 2, $h_2(n)$, the result is shown in Fig. 8. The equalized response in the top plot shows pre-echoes and post-echoes but shortening (compared to $h_2(n)$ depicted below as red plot) to give a correspondingly lower value of $\psi = 2.27$ The magnitude responses are shown on the right.

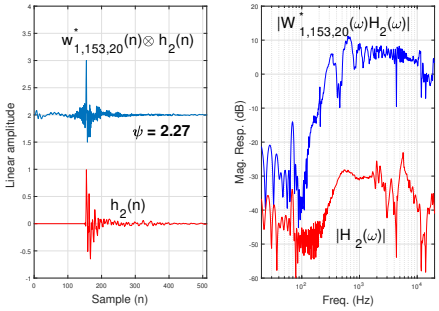


Fig. 8: Filtering performance as an example with a single filter from Fig. 7 convolved with the response at an adjacent position.

5 Results

For each of the transducers in the slot (depicted in Fig. 2a), seventeen measurements were obtained in the horizontal and vertical planes as shown in Fig. 2b. While the algorithm could be employed to design a filter using the combined measurements, one of the objectives of this study was to understand the robustness performance, as well as the strengths and weaknesses, if any, of the approach in each plane. We set the filter order $P = 512$ and the rest of the parameters for (2) were empirically set as $T = 0.3, Q = 150$ samples, $\alpha_1 = 0.3, \alpha_2 = \alpha_3 = 0.2$, and $\alpha_4 = 0.5$. A summary of the results is shown in Table 1 highlighting optimized parameters for both slot-loaded transducers (US: DUT-1, μ: DUT-2) that improve the temporal and magnitude equalization over multiple positions (viz., $\lambda^* > 1$[1]). The results for horizontal directions show improvement in all positions, with the DUT-1 results outperforming

[1]The optimal λ^* is determined by using (i^*,Δ^*,L^*) in (3)-(5)

Table 1: Multi-position Performance

Slot	i^*	Δ^*	L^*	λ^*	ψ^*
DUT-1_{horiz}	4	49	4	17	3183
DUT-2_{horiz}	5	147	20	17	1714
DUT-$1_{\text{vert.}}$	7	144	1	10	884
DUT-$2_{\text{vert.}}$	15	143	7	7	343

the DUT-2. Notably, the final prototype $h_{i^*}(n)$ and the number of optimal iterations L^* that give the optimal filters using the Algorithm and the metrics (3)-(5) are different for both directions and transducer slots. All seventeen measured responses were improved horizontally with the optimal filter for the corresponding slot (viz., $\lambda^* = 17$). For vertical directions, the DUT-1 slot outperformed the DUT-2 regarding the number of positions improved upon and the higher value for the optimized metric ψ^*. Figures 9-11 show examples of high-quality time- and frequency-domain before and after plots (red: measured, blue: equalized with optimum filters with $P = 512$) at example four positions[2]. Figures 12-17 show examples of high-quality time- and frequency-domain before and after plots, as well as plots of relatively least-performing results. While the least-performing equalized results are generally better than the original responses, low-energy pre-echoes result in a less clean, visually observed signal, as predicted by the metrics.

6 Conclusions & Future Directions

This paper presents a new algorithm incorporating a novel metric for performing multiposition time-domain correction of slot-loaded impulse responses. Seventeen positions were measured in the horizontal and vertical directions for two different slot-loaded transducer systems (used in TVs) to assess the effectiveness of the proposed technique. The technique consistently performs well in the horizontal direction while keeping its performance in most positions in the vertical direction. This can be seen from the (λ^*, ψ^*) results in Table 1, and before and after plots in Figs. 9-17. Additionally, the filter delays Δ required to obtain these results are amenable for real-time processing. Future directions include extending the algorithm towards combining all

[2]DUT-2 horizontal magnitude domain results are not shown as they are similarly flat in frequency, and only a subset of plots are shown in the paper for space saving

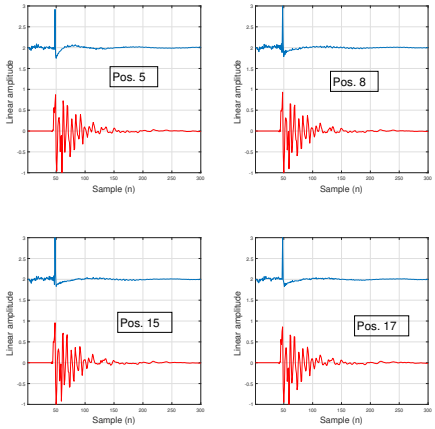


Fig. 9: Example of horizontal time-domain results for DUT-1.

measurements for a single filter over both horizontal and vertical directions, spatial weighting integrated in Eq. (4) to factor the importance of specific responses, assessment of the technique at various filter orders P, pre-processing (e.g., response smoothing) to improve the consistency of performance for all positions, hyperparameter optimization to select parameters $\{i, L, P\}$ and weighting coefficients in the temporal metric, notch correction constraints using perceptual thresholds [38], as well as nonlinear filtering using deep learning.

7 Acknowledgements

The authors thank the members of the DMS Audio Lab, Samsung Research America, and the Visual Display Sound Lab at Samsung (Korea) for supporting this work.

References

[1] ITU-R BS. 2051-3, *Advanced sound system for programme production* , Int. Telecom. Union (ITU), 2022.

[2] S. Bharitkar, "A Comparison Between Sweep Signals for Simultaneous Deconvolution," *Proc. 157th Audio Eng. Soc. Conv.* (AES), June 2024, Madrid (Spain).

[3] F. Toole and S. E. Olive, "The Modification of Timbre by Resonances: Perception and Measurement," *J. Audio Eng. Soc.*, 36, 1988, pp. 122–142.

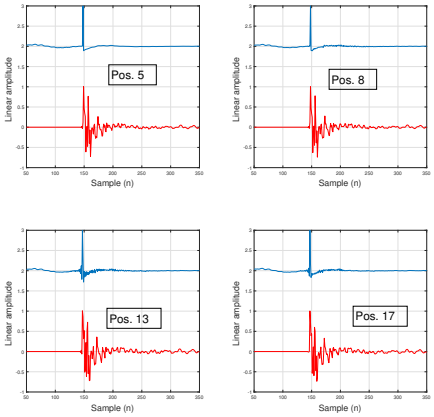


Fig. 10: Example horizontal time-domain results for DUT-2.

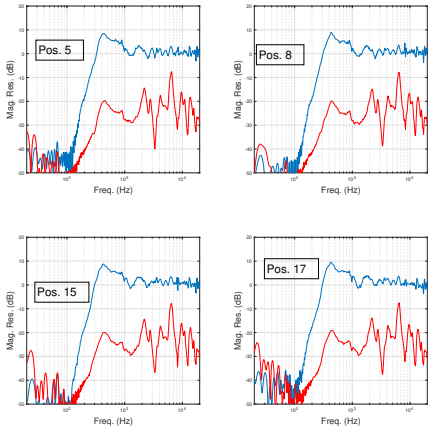


Fig. 11: DUT-1 frequency-domain corresponding to Fig. 9.

[4] J. Vanderkooy, "Aspects of MLS Measuring Systems," *J. Audio Eng. Soc.*, 42(4), April 1994, pp. 503–516.

[5] A. Farina, "Simultaneous Measurement of Impulse Response and Distortion with a Swept-Sine Technique," *Proc. 108th Audio Eng. Soc. (AES) Conv.*, Paris (France), Feb. 2000.

[6] C. Antweiler, A. Telle, and P. Vary, "NLMS-type system identification of MISO systems with shifted perfect sequences," *Proc. IWAENC*, Seattle (USA), 2008.

[7] P. Hatziantoniou and J. Mourjopoulos, "Errors in real-time room acoustics dereverberation," *J. Audio Eng. Soc.*, 52(9), Sept. 2004, pp. 883–899.

[8] P. Hatziantoniou and J. Mourjopoulos, "Generalized fractional-octave smoothing of audio and acoustic responses," *J. Audio Eng. Soc.*, 48(4), Apr. 2000, pp. 259–280.

[9] B. Radlovic and R. Kennedy, "Nonminimum-phase equalization and its subjective importance in room acoustics," *IEEE Trans. Speech & Audio Proc.*, 8(6), Nov. 2000, pp. 728–737.

[10] S. Bharitkar and C. Kyriakakis, *Immersive Audio Signal Processing*, Springer-Verlag, 2006.

[11] S. Cecchi, A. Carini, and S. Spors "Room response equalization-A review," *Appl. Sci.*, 8(16), 2018, pp. 1-47.

[12] M. Karjalainen, P. Esquef, P. Antsalo, A. Mäkivirta, and V. Välimäki, "Frequency-zooming ARMA modeling of resonant and reverberant systems," *J. Audio Eng. Soc.*, 50(12), Dec. 2002, pp. 1012–1029.

[13] B. Bank, "Warped, Kautz, and Fixed-pole parallel filters: A Review," *J. Audio Eng. Soc.*, 70(6), June 2022, pp. 414–434.

[14] P. Clarkson, J. Mourjopoulos, "Spectral, phase, and transient equalization for audio systems," *J. Audio Eng. Soc.*, 33(3), March 1985, pp. 127–132.

[15] R. Greenfield and M. Hawksford, "Efficient filter design for loudspeaker equalization," *J. Audio Eng. Soc.*, 39(10), Oct. 1991, pp. 739–751.

[16] S. Elliott and P. Nelson, "Multiple-point equalization in a room using adaptive digital filters," *J. Audio Eng. Soc.*, 37(11), Nov. 1989, pp. 899–907.

[17] R. Wilson, "Equalization of loudspeaker drive units considering both on- and off-axis responses," *J. Audio Eng. Soc.*, 39(3), March 1991, pp. 127–139.

[18] J. Mourjopoulos, "Digital equalization of room acoustics," *J. Audio Eng. Soc.*, 42(11), Nov. 1994, pp. 884–900.

[19] T. Papadopoulos and P. Nelson, "Computationally efficient inversion of mixed phase plants with IIR

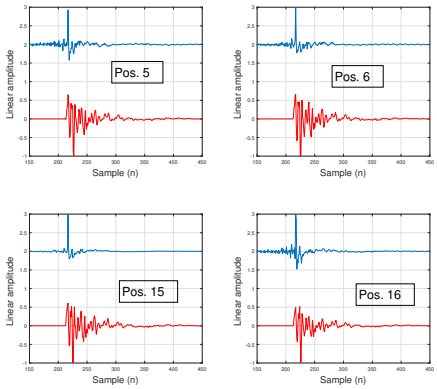


Fig. 12: Subset of good-performing vertical time-domain results for DUT-1.

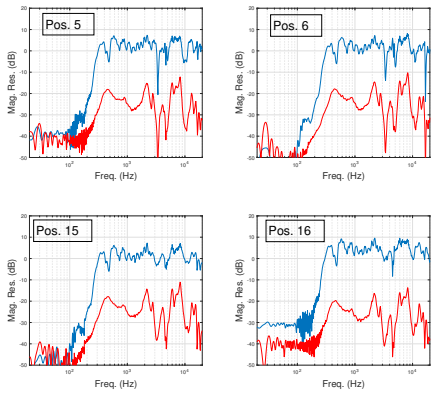


Fig. 13: DUT-1 corresponding to Fig. 12.

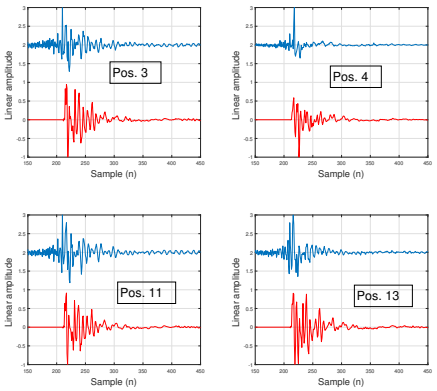


Fig. 14: Least performing vertical results for DUT-1.

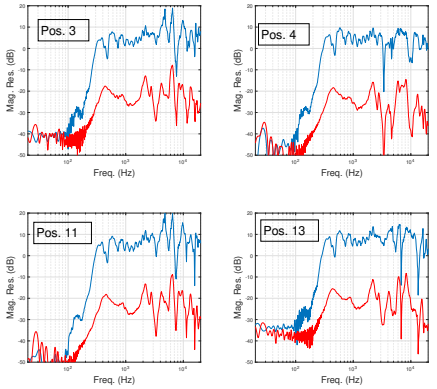


Fig. 15: DUT-1 corresponding to Fig. 14.

filters," *Proc. 113th Audio Eng. Soc. Conv.* (AES), Oct. 2002, Los Angeles (USA).

[20] S. Norcross, G. Soulodre, and M. Lavoie, "Evaluation of inverse filtering techniques for room/speaker equalization," *Proc. 113th Audio Eng. Soc. Conv.* (AES), Oct. 2002, Los Angeles (USA).

[21] S. Norcross, G. Soulodre, and M. Lavoie, "Further investigations of inverse filtering," *Proc. 115th Audio Eng. Soc. Conv.* (AES), Oct. 2003, Los Angeles (USA).

[22] J. Sarris, N. Stefanakis, and G. Cambourakis "Signal processing techniques for robust multichannel sound equalisation," *Proc. 116th Audio Eng. Soc. Conv.* (AES), May 2004, Berlin (Germany).

[23] S. Norcross, G. Soulodre, and M. Lavoie, "Distortion audibility in inverse filtering," *Proc. 117th Audio Eng. Soc. Conv.* (AES), Oct. 2004, San Francisco (USA).

[24] A. Marques and D. Freitas, "Comparison of inverse filter real-time equalization methods for non-minimum phase loudspeaker systems," *Proc. 117th Audio Eng. Soc. Conv.* (AES), Oct. 2004, San Francisco (USA).

[25] G. Ramos and J. Lopez, "Filter design method for loudspeaker equalization based on IIR parametric

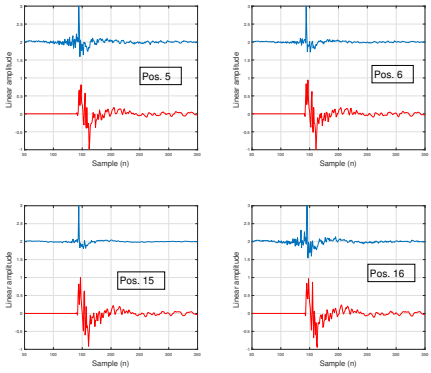


Fig. 16: Subset of good-performing vertical results for DUT-2.

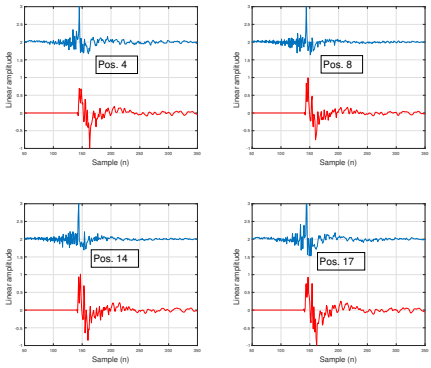


Fig. 17: Least performing vertical results for DUT-2.

filters," *J. Audio Eng. Soc.*, 54(12), Dec. 2006, pp. 1162–1178.

[26] A. Primavera, S. Cecchi, F. Piazza, and A. Carini, "Mixed time-frequency approach for multipoint room response equalization," *Proc. 45th Audio Eng. Soc. Conf.* (AES), 2012, Helsinki (Finland).

[27] S. Cecchi, M. Virgulti, S. Doria, F. Bettarelli, and F. Piazza, "Development of multipoint mixed-phase equalization system for multiple environments," *Proc. 134th Audio Eng. Soc. Conv.* (AES), 2013, Rome (Italy).

[28] A. Mäkivirta, J. Liski, and V. Välimäki, "Modeling and delay-equalizing loudspeaker responses," *J. Audio Eng. Soc.*, 66(11), Nov. 2018, pp. 922–934.

[29] V. Staggs, "Transient-response equalization of sealed-box loudspeakers," *J. Audio Eng. Soc.*, 30(12), Dec. 1982, pp. 906–911.

[30] R. Stroud, "Quasi-anechoic loudspeaker measurement using notch equalization for impulse response shortening," *Proc. 129th Audio Eng. Soc. Conv.* (AES), 2010, San Francisco (USA).

[31] S. Schlecht, T. Sinjanakhom, and V. Välimäki, "Multi-shelf graphic equalizer," *Sig. Proc.*, 226, July 2024, pp. 1–8.

[32] J. Mourjopoulos, P. Clarkson, and J. Hammond, "A comparative study of least-squares and holomorphic techniques for the inversion of mixed-phase signals," *Proc. ICASSP*, May 1982, Paris (France).

[33] S. Neely and J. Allen, "Invertibility of a room impulse response," *J. Acoust. Soc. Amer.*, 66(1), July 1979, pp. 165–169.

[34] D. Preis, "Phase distortion and phase equalization in audio signal processing-A tutorial review," *J. Audio Eng. Soc.*, 30(11), Nov. 1982, pp. 774–794.

[35] S. Herzog and M. Hilsamer, "Low frequency group delay equalization of vented boxes using digital correction filters," *Proc. 17th Int. Conf. Digital Audio Effects* (DAFx), Sept. 2014, Erlangen (Germany).

[36] O. Kirkeby, P. Nelson, H. Hamada, and F. Orduna-Bustamante, "Fast deconvolution of multichannel systems using regularization," *IEEE Trans. Speech & Audio Proc.*, 6(2), March 1998, pp. 189–194.

[37] A. Oppenheim and R. Schafer, *Discrete-Time Signal Processing*, Prentice-Hall, Aug. 2009.

[38] S. Bharirtkar, C. Robinson, and A. Poulain,"Equalization of Spectral Dips Using Detection Thresholds," *Proc. 140th Audio Eng. Soc. Conv.* (AES), June 2016, Paris (France).